Persistent growth of microtubules at low density

Anton Burakov[a,b,†], Ivan Vorobjev[a,b,c,†], Irina Semenova[a], Ann Cowan[a], John Carson[a], Yi Wu[a], and Vladimir Rodionov[a,*]

[a]R.D. Berlin Center for Cell Analysis and Modeling and Department of Cell Biology, UConn Health, Farmington, CT 06030; [b]A.N. Belozersky Institute of Physico-Chemical Biology, Lomonosov Moscow State University, Moscow 119992, Russia; [c]Department of Biology, School of Sciences and Humanities and National Laboratory Astana, Nazarbayev University, 010000 Nur-Sultan, Kazakhstan

ABSTRACT **Microtubules (MTs) often form a polarized array with minus ends anchored at the centrosome and plus ends extended toward the cell margins. Plus ends display behavior known as dynamic instability—transitions between rapid shortening and slow growth. It is known that dynamic instability is regulated locally to ensure entry of MTs into nascent areas of the cytoplasm, but details of this regulation remain largely unknown. Here, we test an alternative hypothesis for the local regulation of MT behavior. We used microsurgery to isolate a portion of peripheral cytoplasm from MTs growing from the centrosome, creating cytoplasmic areas locally depleted of MTs. We found that in sparsely populated areas MT plus ends persistently grew or paused but never shortened. In contrast, plus ends that entered regions of cytoplasm densely populated with MTs frequently transitioned to shortening. Persistent growth of MTs in sparsely populated areas could not be explained by a local increase in concentration of free tubulin subunits or elevation of Rac1 activity proposed to enhance MT growth at the cell leading edge during locomotion. These observations suggest the existence of a MT density–dependent mechanism regulating MT dynamics that determines dynamic instability of MTs in densely populated areas of the cytoplasm and persistent growth in sparsely populated areas.**

Monitoring Editor
Antonina Roll-Mecak
National Institutes of Health, NINDS

Received: Aug 20, 2020
Revised: Dec 8, 2020
Accepted: Jan 6, 2021

INTRODUCTION

Cytoplasmic microtubules (MTs) play essential roles in spatial organization of the cytoplasm (Lane and Allan, 1998), intracellular transport (Vale, 2003; Welte, 2004; Caviston and Holzbaur, 2006), cell locomotion (Wittmann and Waterman-Storer, 2001; Etienne-Manneville, 2013), and mitosis (Walczak and Heald, 2008; Heald and Khodjakov, 2015). MTs are often organized into polarized arrays with minus ends clustered at a MT-organizing center, such as the centrosome, and plus ends extended toward the cell periphery. MTs in these arrays are highly dynamic and rapidly turn over by addition and loss of tubulin subunits at the ends. Turnover of tubulin subunits occurs by two independent mechanisms, known as minus- and plus-end pathways. The minus-end pathway entails release of MTs from the centrosome and their rapid disassembly through loss of tubulin subunits from minus ends (Keating *et al.*, 1997). The plus-end pathway involves alternating phases of addition or loss of tubulin subunits at the plus ends. MT plus ends either slowly grow or rapidly shorten and undergo sudden transitions from growth to shortening (catastrophe) or from shortening to growth (rescue) (Mitchison and Kirschner, 1984). This behavior, known as dynamic instability, allows MT plus ends to explore intracellular space and to make contacts with membrane organelles (Lomakin *et al.*, 2009), kinetochores of chromosomes (Hayden *et al.*, 1990), and the plasma membrane (Akhmanova *et al.*, 2001).

Dynamic instability of MTs is regulated by many different protein factors that alter various aspects of MT plus-end growth or shortening (Desai and Mitchison, 1997; Holmfeldt *et al.*, 2009; van der Vaart *et al.*, 2009; Akhmanova and Steinmetz, 2015; Goodson and Jonasson, 2018). MT-stabilizing factors promote net MT assembly by preventing catastrophes, increasing frequency of rescue events or decreasing MT shortening rates. Likewise, MT-destabilizing factors

This article was published online ahead of print in MBoC in Press (http://www.molbiolcell.org/cgi/doi/10.1091/mbc.E20-08-0546) on January 13, 2021.

†These authors contributed equally to this work.

*Address correspondence to: Vladimir Rodionov (rodionov@ uchc.edu).

Abbreviations used: FCS, fluorescence correlation spectroscopy; MT, microtubule.

© 2021 Burakov, Vorobjev, *et al*. This article is distributed by The American Society for Cell Biology under license from the author(s). Two months after publication it is available to the public under an Attribution–Noncommercial–Share Alike 3.0 Unported Creative Commons License (http://creativecommons.org/licenses/by-nc-sa/3.0).

"ASCB®," "The American Society for Cell Biology®," and "Molecular Biology of the Cell®" are registered trademarks of The American Society for Cell Biology.

stimulate MT disassembly by inducing opposite changes in key parameters of MT dynamic instability. Protein–protein interactions responsible for activities of many protein factors that regulate MT dynamics have been studied at a great level of detail in vitro, and in many cases it is now clear how individual proteins modulate specific aspects of MT dynamic instability (Akhmanova and Steinmetz, 2015). However, how protein factors work together in vivo to alter MT dynamics at global and local scales remains largely unknown.

One of the most dramatic examples of altered MT dynamics is provided by cytoplasmic fragments and cytoplasts lacking the centrosome. Our past work showed that in the absence of the centrosome, MTs turn over by net loss of subunits from free minus ends and net addition of subunits to the plus ends (the pattern of turnover known as treadmilling). Remarkably, in marked contrast to intact cells, plus ends of treadmilling MTs in cytoplasmic fragments continuously grow or pause but never shorten (Rodionov and Borisy, 1997a; Rodionov *et al.*, 1999). To explain the lack of MT catastrophes, we proposed a mechanism based on the concentration of free tubulin subunits (Rodionov *et al.*, 1999). We suggested that loss of MT attachment to the centrosome and shortening of minus ends results in a shift of the steady-state level of MT assembly toward a decreased level of polymer and an increased level of free tubulin subunits. Increased concentration of free tubulin subunits would lower the probability of catastrophes at plus ends of remaining MTs, thus promoting their persistent growth (Rodionov *et al.*, 1999).

In our hypothesis, the key factor that determines switching of plus-end dynamics from dynamic instability to persistent growth is elevated levels of free tubulin subunits. However, removal of the centrosome also reduced the amount of MT polymer in cytoplasmic fragments (Rodionov *et al.*, 1999). Therefore an alternative hypothesis is that the pattern of plus-end dynamics is influenced by the density of the MT polymer pool. In this study, we test whether the density of the MT polymer pool influences MT behavior by locally depleting MTs in the cytoplasm without changing the concentration of free tubulin subunits. Contrary to predictions of the free tubulin hypothesis, we found a dramatic effect of the MT polymer pool. In experimentally produced areas of cytoplasm sparsely populated with MTs, plus ends persistently grew or paused and rarely shortened, whereas growing plus ends that entered regions of the cytoplasm densely populated with MTs acquired catastrophes. Our observations suggest a new mechanism for regulation of MT dynamics that couples plus-end dynamics to MT density.

RESULTS

Persistent growth of MTs in cytoplasmic fragments and cytoplasts lacking the centrosome could be explained by increased concentration of free tubulin subunits or by reduced levels of MT polymer. To determine whether behavior of MT plus ends depends on MT polymer levels, we examined MT dynamics in regions of the cytoplasm with reduced MT density. To locally deplete peripheral cytoplasm of MTs, we introduced a barrier between the centrosome and the cell periphery by microsurgical manipulation with a thin glass microneedle. The manipulation converted the intact cell into one with toroidal topology containing an elongated barrier hole parallel to the cell margin. Because the barrier would cut off cytoplasmic space from "line-of-site" connection to the centrosome, we expected that the density of MTs distal to the barrier should be significantly reduced compared with the rest of the peripheral cytoplasm.

To test whether MT density distal to the barrier was indeed reduced, we acquired live fluorescence images of MTs in the manipulated cells. For these experiments, we used fish (black tetra) melanophores. These cells contain thousands of pigment granules that rapidly aggregate in the cell center or disperse throughout the cytoplasm in response to hormonal stimuli (Murphy and Tilney, 1974; Rodionov *et al.*, 1991). The unusually large size (~200 μm) of black tetra melanophores makes them ideally suitable for experiments that involve microsurgery (Rodionov and Borisy, 1997a,b). Furthermore, MTs in these cells are numerous, and their plus ends display robust dynamic instability (Rodionov *et al.*, 1994). For fluorescence labeling of MTs, we injected melanophores with tubulin subunits tagged with Cy3, applied pigment aggregation stimuli to clear peripheral cytoplasm of pigment granules that could interfere with live imaging of MTs, and produced a crescent-shaped barrier with the convex surface facing the cell center (Figure 1A, left panel). Microsurgery severed MTs and led to their rapid disassembly in the area of the cytoplasm distal to the barrier through rapid shortening of the nascent minus ends. Imaging of MTs performed 20–30 min after microsurgery showed that MT density distal to the barrier was dramatically reduced (Figure 1A, right panel).

To determine whether MT density distal to the barrier was comparable to the density of MTs in cytoplasmic fragments of melanophores, we traced individual MTs in fluorescence images of peripheral cytoplasm in manipulated cells and cytoplasmic fragments of melanophores that were generated as described previously (Rodionov and Borisy, 1997a). We found that in intact control cells average MT density at the cell margin was 4.31 ± 1.35 μm/μm^2 (mean ± SD, n = 10). MT density in microsurgically produced fragments of melanophores was about fourfold lower (0.96 ± 0.17 μm/μm^2; mean ± SD, n = 10). Remarkably, MT density distal to barriers was comparable to MT density in melanophore fragments (0.92 ± 0.31 μm/μm^2; mean ± SD, n = 10) (Figure 1B). We conclude that isolation of peripheral cytoplasm with a microsurgically produced barrier reduced MT density to levels seen in cytoplasmic fragments lacking the centrosome.

To determine whether MT depletion changed the dynamic behavior of MT plus ends, we acquired time sequences of images of fluorescently labeled MTs in the same cells in sparsely populated areas distal to the barrier and at the cell margin in intact cytoplasm densely populated with MTs. We found that, as expected, in densely populated areas of the cytoplasm, MT plus ends grew and shortened and therefore displayed typical dynamic instability (Figure 1C, left panel; Supplemental Video S1). In striking contrast to the rest of the cytoplasm, plus ends of MTs located distal to the barrier continuously grew or paused but almost never shortened (Figure 1C, right panel) even when they reached the cell margin (Figure 1C, right panel, right column; Supplemental Videos S1 and S2). Continuous growth of MT plus ends distal to the barrier was strikingly similar to persistent MT growth that we previously observed in cytoplasmic fragments of melanophores (Rodionov and Borisy, 1997a).

To quantify regional differences in dynamic behavior of MT plus ends, we tracked plus ends of individual MTs and generated frequency histograms of MT growth rates defined as displacement within 3 s time intervals. We found that the frequency of negative values of MT growth rates, which corresponded to catastrophes, was significantly reduced in MT-depleted regions located distal to the barrier compared with intact densely populated cytoplasm (Figure 1D). Direct quantification of the frequency of MT catastrophes, which we defined as a decrease in MT length for ≥0.5 μm, showed that it was much lower in MT-depleted regions (0.2/min) compared with regions filled with MTs (1.55/min). Furthermore, the frequency of long (≥2.0 μm) catastrophes distal to the barrier was reduced even more significantly (~50-fold, from 0.42/min to 0.008/min). MT rescues that followed catastrophes were also sparse. We conclude that local MT depletion in fish melanophores correlated

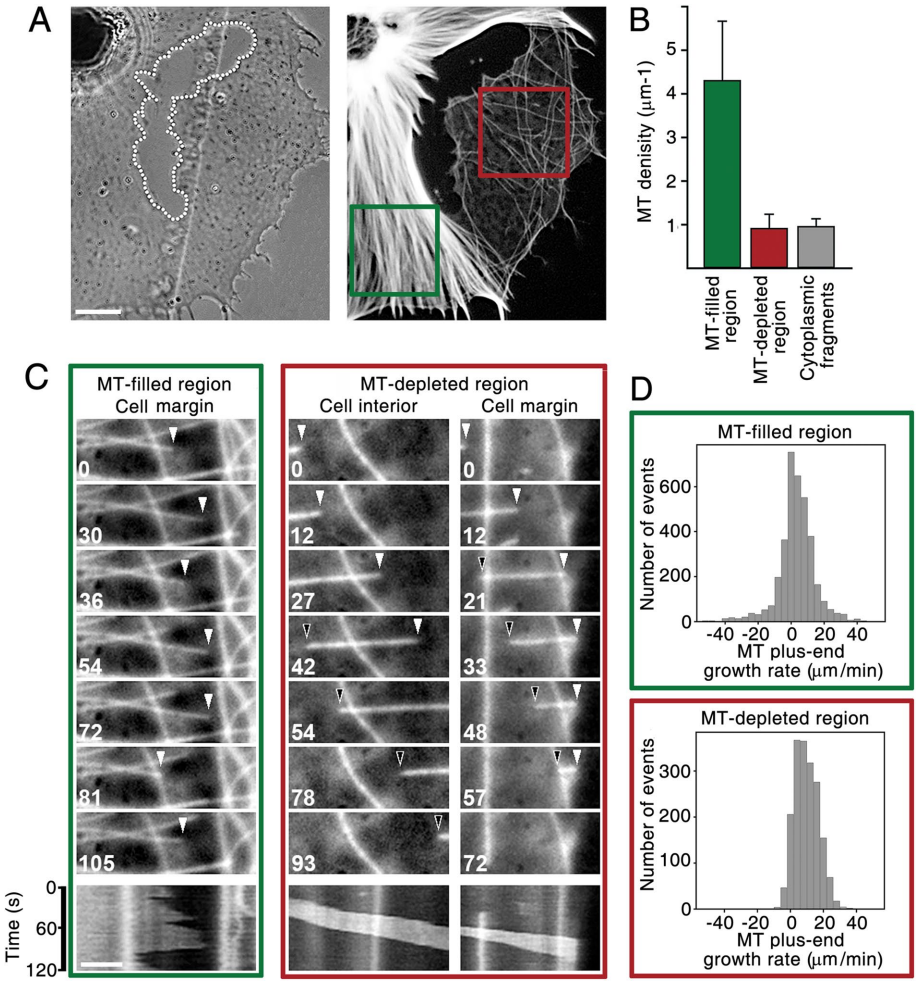

FIGURE 1: A local decrease in MT density in fish melanophores correlates with a reduction in frequency of catastrophes at the MT plus ends. (A) Images of a melanophore with a barrier placed parallel to the cell margin. Left, phase contrast image; right, fluorescence image of MTs. The barrier is outlined with a dotted line in the left image. Color squares in the right-hand image define positions of MT-filled (green) and MT-depleted (red) areas of the cytoplasm used for quantification of MT density (panel B) and dynamics of MT plus ends (panels C and D). MTs are significantly less abundant behind the barrier than at the original cell margin. Bar, 20 μm. (B) Quantitation of MT densities at the cell periphery (left, green bar), in MT-depleted areas distal to the barrier (middle, red bar), and in cytoplasmic fragments of melanophores (right, gray bar). The barrier isolates peripheral cytoplasm from growth of centrosomal MTs and reduces the local density of MTs to levels observed in cytoplasmic fragments. (C) Time sequences of MTs in a densely populated area of the cytoplasm (left panel) and a sparsely populated area distal to the barrier (right panels). Top panels, sequential images of MTs; bottom panels, kymographs. Numbers indicate time in seconds; white arrowheads point to plus ends, and black arrows point to minus ends of MTs. Bar, 5 μm. In a densely populated area, the MT plus end grows and shortens, whereas in a sparsely populated area the MT plus end never shortens even when it reaches the cell margin. (D) Histograms of MT growth rates (measured as displacement of MT plus ends within 3 s time intervals) in areas of cytoplasm densely (top) or sparsely (bottom) populated with MTs. Negative values of growth rates are frequent in densely populated but not in sparsely populated areas.

with a dramatic drop in the frequency of catastrophes of MT plus ends, leading to their persistent growth.

Switching MT plus ends from dynamic instability to persistent growth after MT depletion could be a specific property of melanophores or a common property of the cytoplasm of animal cells. To test whether our observations have general importance, we sought to isolate peripheral cytoplasm from global MT growth in mammalian fibroblasts and selected a common cell line (NIH3T3) for these experiments. We found, however, that because of their small size NIH3T3 fibroblasts did not survive microsurgery well. To improve the survival rate, we increased cell size by treating fibroblasts with mitomycin C—an antitumor antibiotic that blocks cell division without preventing cell growth. After a few days of mitomycin C treatment, the size of NIH3T3 cells increased approximately four- to fivefold, and their survival rate after microsurgery significantly improved as well. Time sequences of images of MTs in mitomycin C–treated cells injected with Cy3-labeled tubulin showed that, again, MTs persistently grew into MT-depleted areas located distal to the barrier but, as expected, displayed robust dynamic instability elsewhere at the cell periphery (Supplemental Figure 1, top and middle). Tracking MT plus ends revealed a significant shift of MT growth frequency histograms to positive values in MT-depleted areas (Supplemental Figure 1, bottom). The frequency of MT catastrophes (defined as reduction in MT length for ≥0.5 μm) was dramatically decreased in areas of cytoplasm distal to the barrier (from 0.543/min to 0.026/min). Furthermore, similar to melanophores, in fibroblasts MT plus ends in sparsely populated areas never underwent catastrophes upon reaching the cell margin (Supplemental Figure 1, middle right panel, right column). Similar changes in MT dynamic behavior were also observed in normal human skin fibroblasts (Supplemental Video S3). We conclude that persistent growth of MT plus ends into sparsely populated regions of the cytoplasm is a general property of animal cells.

The frequency of MT catastrophes is known to decline with increasing concentration of free tubulin subunits (Walker *et al.*, 1988). Therefore the reduced frequency of MT catastrophes observed in sparsely populated areas of the cytoplasm could be explained by a local increase in the concentration of free tubulin subunits. Computational modeling suggests that the existence of a gradient of tubulin subunit concentration within the cytoplasm is an unlikely possibility (Odde, 1997) because of the fast rate of tubulin diffusion (Salmon *et al.*, 1984; Wang *et al.*, 2004). Nevertheless we tested this possibility experimentally by comparing concentrations of free tubulin subunits in areas of low MT density located distal to the barrier to areas of high MT density at the intact cell margin. To compare tubulin concentrations, we first measured tubulin fluorescence in regions between MTs in images of melanophores injected with tubulin subunits labeled with Cy3 (Figure 2A). Cy3 fluorescence was normalized for fluorescence of the volume marker Alexa Fluor 488–labeled dextran that was coinjected with Cy3 tubulin (Figure 2A, bottom panel). The normalized Cy3

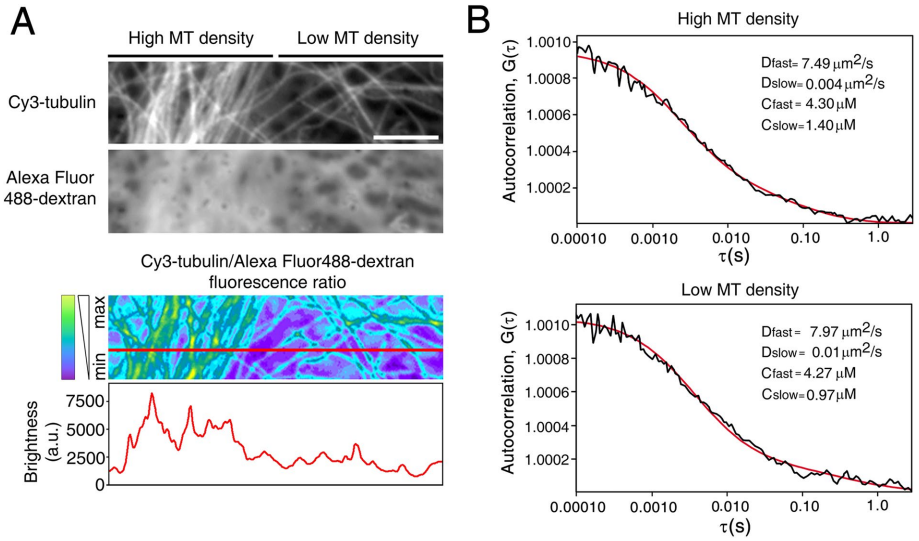

FIGURE 2: Concentrations of free tubulin subunits are similar in regions of cytoplasm with high and low MT density. (A) Ratiometric fluorescence imaging. Fluorescence images of a melanophore coinjected with cell volume marker Alexa 488–dextran and Cy3-tubulin. From top to bottom, high-magnification fluorescence images of a transition zone between high and low MT density regions of cytoplasm in Cy3 channel, Alexa 488 channel, and a ratiometric Cy3/Alexa 488 image. Bottom panel shows fluorescence intensity profile measured along the line shown in red in the ratiometric image. The values of gray levels between MTs in the ratiometric image, which reflect the concentration of free tubulin subunits, are similar in areas of the cytoplasm with high and low MT densities. Bar, 5 μm. (B) FCS analysis of EGFP–tubulin in an NIH3T3 fibroblast. The two panels show representative FCS measurements in the high MT density region (top panel) and in the low MT density region (bottom panel) in the same cell. The black lines show the autocorrelation functions for EGFP–tubulin plotted vs. τ in a log scale. The red lines show fitted curves using a two-component model consisting of a major component with fast τ value (likely corresponding to freely diffusing tubulin subunits) and a minor component with a slower τ value (possibly corresponding to tubulin molecules bound to slow or immobile partners). The total number of fluorescent molecules in the FCS volume and the relative proportions of molecules with fast and slow τ values were determined at each location. The concentrations of fast and slow (C_{fast} and C_{slow}) components were derived from the number of fast and slow component molecules in the FCS volume, and the diffusion coefficients for the fast and slow components (D_{fast} and D_{slow}) were derived from the fast and slow τ values as described in *Materials and Methods*. The concentrations of fast component molecules, likely corresponding to freely diffusing tubulin subunits, are similar in high and low MT density regions.

fluorescence measured in interstices between MTs in areas of cytoplasm with sparse MTs (distal to the barrier) was comparable to that in areas with high MT density (ratio = 0.83 ± 0.17, mean ± SD, n = 17). This result suggests that, as expected, the concentration of free tubulin subunits is not significantly increased in areas of cytoplasm with low MT density. However, it is possible that fluorescence measured at the cell margin densely populated with MTs overestimated the amount of labeled free tubulin and therefore the fluorescence ratio may have been underestimated in these regions. Furthermore, it is also possible that the total normalized fluorescence measured in these experiments represents both freely diffusing tubulin subunits and slowly diffusing tubulin species associated with less mobile cytoplasmic components.

To test these possibilities, local concentrations and diffusion coefficients for enhanced green fluorescent protein (EGFP)-labeled tubulin were analyzed using fluorescence correlation spectroscopy (FCS). EGFP-labeled tubulin was expressed in mitomycin-treated NIH3T3 fibroblasts, and after microsurgery, FCS measurements were performed with the observation volume positioned at two separate locations within the region of the cytoplasm with high MT density and at two separate locations within the region of cytoplasm with low MT density, in seven different cells. The FCS autocorrelation functions determined at each location were fitted to determine the concentrations and diffusion coefficients for exogenous fluorescent EGFP–tubulin molecules in the corresponding regions (see Figure 2). The level of expression of exogenous EGFP–tubulin varies from cell to cell; however, within each cell the concentrations and diffusion coefficients of exogenous EGFP–tubulin at different locations are presumably proportional to the concentrations and diffusion coefficients of unlabeled endogenous tubulin at the corresponding locations. The results reveal two distinct tubulin components with different τ values. The fraction of major (fast) component (0.67 ± 0.12; mean ± SD, n = 28 measurements) likely represents freely diffusing EGFP–tubulin molecules. The nature of the minor (slow) component (0.33 ± 0.12; mean ± SD, n = 28 measurements) is not known. It may represent tubulin subunits bound to slowly diffusing cytoplasmic components or tubulin subunits reversibly associating with and dissociating from immobile cytoplasmic structures. Concentrations and diffusion coefficients for fast and slow components were as follows: (fast component concentration = 1.68 ± 0.25 μM, mean ± SD, n = 28 measurements in seven different cells; fast component diffusion coefficient = 12.6 ± 6.3 $\mu m^2/s$, mean ± SD, n = 28 measurements in seven different cells; slow component concentration = 0.84 ± 0.25 μM, mean ± SD, n = 28 measurements in seven different cells; slow component diffusion coefficient = 0.003 ± 0.004 $\mu m^2/s$, mean ± SD, n = 28 measurements in seven different cells). Cell-to-cell variation in concentrations and diffusion coefficients was larger than location-to-location variation within individual cells. For the fast component, which likely represents free tubulin, the ratio of concentrations between high MT/low MT regions was 1.008 ± 0.49, mean ± SD, n = 7 cells, and the ratio of diffusion coefficients between high MT/low MT regions was 0.97 ± 0.15, mean ± SD, n = 7 cells). Because both these ratios are close to 1, this indicates that the observed differences in MT catastrophe frequency between regions with low and high MT densities are not attributable to local differences in free tubulin subunit concentrations or diffusion coefficients.

The results of our experiments reveal a striking correlation between the frequency of catastrophes and MT density that could not be attributed to local changes in concentration of free tubulin subunits. This suggests a novel mechanism that dictates uninterrupted growth of MT plus ends in sparsely populated areas of cytoplasm and switching between growth and shortening in densely populated areas. If such a mechanism exists, MT plus ends should undergo catastrophes after they enter a densely populated area of the cytoplasm. We scrutinized our time-lapse sequences for instances of such entry but due to the inherently low MT density and random orientation of MTs distal to the barrier, episodes of MT growth toward densely populated areas of the cytoplasm were vanishingly

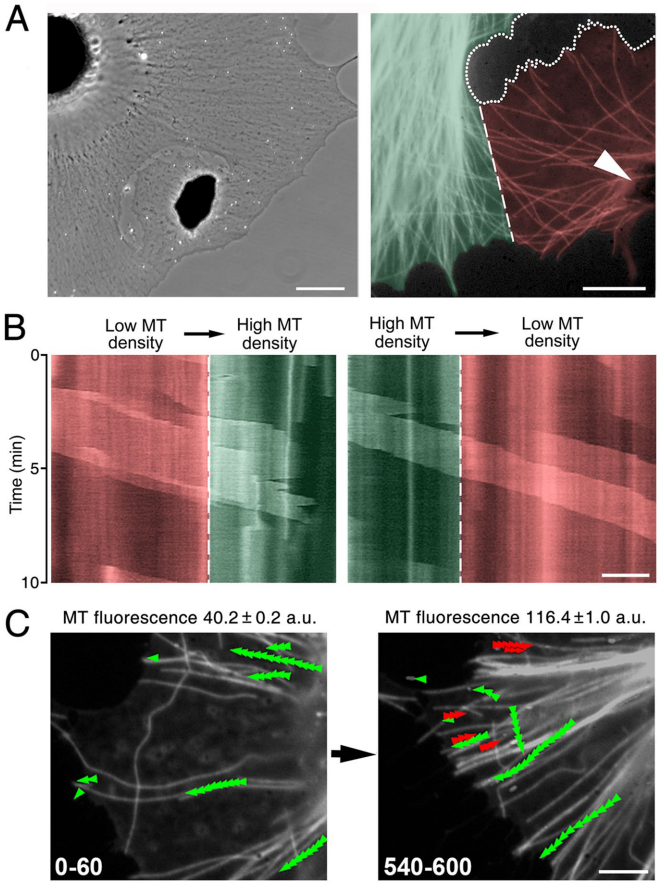

FIGURE 3: Catastrophe frequency depends on local density of MTs. (A) Design of an experiment for detecting transitions of growing MT ends between areas of cytoplasm with different densities of MTs. To increase the probability of entering a high MT density area, an artificial MT-organizing center was created by local aggregation of pigment granules distal to the microsurgically generated wound. The ectopic pigment granule aggregate nucleated MTs that grew in random directions including into a high MT density area. Left, phase contrast image of a cell with an ectopic pigment granule aggregate formed distal to the barrier; right, fluorescence image of MTs in proximity to the ectopic aggregate; dashed line depicts the border between high (green background) and low (red background) MT density areas; arrowhead indicates the position of the ectopic pigment granule aggregate; a dotted line defines margins of the barrier; images were acquired approximately 20 min after stimulation of pigment granule aggregation. Bars, 10 μm. Numerous MTs connected to the ectopic pigment granule aggregate are oriented toward the high MT density area. (B) Kymographs of MT ends growing into high (left panel) or low (right panel) MT density areas. Areas of high and low MT densities are highlighted in green and red, respectively, and the border between them is defined by the dashed line. MTs tips that persistently grow in the low MT density area acquire catastrophes after entering the high MT density area (left panel). Likewise, MT ends that occasionally shorten in the high MT density area switch to uninterrupted growth after transiting into a low MT density area. Bar, 5 μm. (C) Fluorescence images of MTs acquired in the same area behind the barrier soon after microsurgery (left panel) or 10 min after the acquisition of the first time series (right panel). Each panel shows the final images of 60 s time sequences. Green sets of arrowheads depict shortening minus ends and red sets shortening plus ends of MTs. Numbers shown at the top of each panel are values for averaged fluorescence signal from MTs, providing a measure for their density. A 2.9-fold increase in MT density correlates with the appearance of shortening plus ends of MTs. Bar, 5 μm.

rare. To increase frequencies of transitions of MT tips between areas of low and high MT densities, we directed MT growth by taking advantage of the ability of melanophores to form local aggregates of pigment granules that serve as ectopic MT-organizing centers (Rodionov and Borisy, 1997a; Vorobjev *et al.*, 2001). We performed microsurgery on cells with dispersed pigment granules and induced pigment granule aggregation. While the bulk of pigment granules rapidly moved to the cell center along centrosomal MTs, those pigment granules that were isolated by the barrier formed a local pigment aggregate (Figure 3A, arrowhead; Supplemental Video S4). Live fluorescence imaging showed that, as expected (Rodionov and Borisy, 1997a), new MTs continuously emerged from the local granule aggregate and grew in random directions, including the area of high MT density. Remarkably, we found that as soon as MT plus ends entered areas of high MT density they began to undergo multiple long catastrophes (Figure 3B, left panel; Supplemental Video S5). Conversely, we found that shortening events completely disappeared when MT plus ends grew from high into low MT density regions (Figure 3B, right panel; Supplemental Video S5).

These observations support our hypothesis that local MT density determines the pattern of plus-end dynamics, but they do not rule out the possibility that dramatic changes in behavior of MT plus ends depend on structural differences of the cytoplasm in low and high MT density regions, rather than on MT density itself. In particular, continuous growth of MTs distal to barriers could result from reduced levels of obstacles in the way of polymerizing MT tips. Indeed, in vitro studies indicate that growing MT plus ends undergo force-induced catastrophes when stalled at microfabricated walls (Janson *et al.*, 2003). In animal cells, forces generated by polymerizing MTs that encounter a dense meshwork of actin filaments are likely responsible for increased catastrophe rates seen at the cell margins. Therefore it was possible that the inhibition of catastrophes observed in our experiments could be explained by a reduced density of actin filaments in regions of cytoplasm distal to the barriers. To test this possibility, we compared the densities of actin filaments in regions distal to barriers and intact cell margins. We injected mitomycin-treated NIH3T3 cells with Oregon Green 488 dextran, which served as an intracellular volume marker, performed microsurgery to create a barrier, and stained cells with tetramethylrhodamine (TRITC)-labeled phalloidin, which selectively binds to polymerized actin filaments. We found that TRITC/Oregon Green 488 fluorescence ratios measured in seven cells is always higher in regions of cytoplasm distal to barriers (Supplemental Figure 2). Therefore continuous growth of plus ends in low MT density regions cannot be explained by a reduced density of actin filaments. Furthermore, we also noticed that in some melanophores centrosomal MTs gradually fill areas of low MT density during prolonged incubation after microsurgery. Strikingly, in such cells, tips of "pioneer" MTs persistently grow into sparsely populated areas but as MT density increases, MT tips begin to undergo vigorous catastrophes (Figure 3C; Supplemental Video S6). Thus, transition from persistent growth to dynamic instability occurred in the same region of cytoplasm. Taken together, these results indicate that changes in dynamic behavior of MT plus ends cannot be explained by local variations in the organization of the cytoplasm inflicted by the creation of the barrier.

MT plus ends display dynamic instability at high local MT density but switch to continuous growth if the density drops. Such switching allows MTs to rapidly fill newly formed regions of cytoplasm that emerge during cell growth or migration. In migrating cells, MTs that enter the leading lamella experience fewer catastrophes and spend more time growing than MTs that terminate farther from the leading edge (Waterman-Storer and Salmon, 1997; Wadsworth, 1999). Local

growth of MTs is regulated by small GTPase Rac1 (Wittmann *et al.*, 2003) that recruits and activates downstream effector proteins, such as p21-activated kinase 1 (Pak1) (Dharmawardhane *et al.*, 1999; Sells *et al.*, 2000). Rac1 effectors in turn reduce the activities of protein factors destabilizing MTs (Daub *et al.*, 2001; Wittmann *et al.*, 2004; Braun *et al.*, 2014) and increase the activities of MT-stabilizing factors (Wittmann and Waterman-Storer, 2005; Kumar *et al.*, 2009), leading to net MT growth at the advancing cell leading edge. While most of our experiments used fish melanophores that never move across the substrate, we nonetheless tested whether persistent growth of MTs into areas of low MT density seen in manipulated cells involves local activation of Pak1 and depends on the activity of Rac1. We examined the distribution of enzymatically active Pak1 in mitomycin-treated NIH3T3 fibroblasts and investigated the dynamics of MT plus ends in areas of reduced MT density in melanophores during inhibition of Rac1.

To study the distribution of active Pak1 in NIH3T3 fibroblasts, we immunostained manipulated cells with phospho-Pak1 antibody (phospho-S199/204) that binds the active form of the enzyme (Knaus and Bokoch, 1998; Gatti *et al.*, 1999; Chong *et al.*, 2001). Our previous work showed that immunostaining NIH3T3 cells with this antibody revealed a dramatic increase in fluorescence in areas of cytoplasm with locally activated Rac1 (Wu *et al.*, 2009). Therefore the phospho-Pak antibody is suitable for detecting the distribution of active Pak1 in the cytoplasm of NIH3T3 fibroblasts. To compare levels of phosphorylated Pak1 in MT-filled and MT-depleted areas of the cytoplasm, we triple-immunostained manipulated cells with antibodies against tubulin (to detect areas of low MT density distal to the wound), phospho-Pak1 (to quantify phospho-Pak1 fluorescence), and soluble protein glyceraldehyde-3-phosphate dehydrogenase (GAPDH; to normalize phospho-Pak1 fluorescence to the volume of the cytoplasm). Line scans of phospho-PAK1 fluorescence did not reveal a significant increase in levels of phosphorylated Pak1 in areas of low MT density located distal to the barrier (Figure 4A, left panel). Quantification of fluorescence also showed that phospho-Pak1 to GAPDH fluorescence ratios were similar in MT-filled and MT-depleted areas of the cytoplasm (Figure 4A, right panel). These data suggest that the activation of Rac1 effector Pak1 is not involved in stimulating continuous growth of MT plus ends in MT-depleted areas of the cytoplasm.

To directly test whether Rac1 activity was required for processive MT growth in areas of cytoplasm with low MT density, we examined plus-end dynamics in melanophores while inhibiting Rac1 activity. To inhibit Rac1, we treated cells with the membrane-permeable selective Rac1 inhibitor NSC 23766 (Gao *et al.*, 2004) or injected them with a recombinant mutant form of Rac1 protein $Rac1^{N17}$(Ridley *et al.*, 1992), known to have a dominant-negative effect on Rac1activity (Ridley *et al.*, 1992; Waterman-Storer *et al.*, 1999). We found that Rac1 inhibitors did not cause any significant changes in cell shape or plasma membrane activity (unpublished data). This result was not surprising given that the actin cytoskeleton is known to play a minor role in control of the shape of fish melanophores (Rodionov *et al.*, 1998). NSC 23766 treatment induced gradual dispersion of pigment granules, which is likely explained by off-target effect(s) on the cAMP signaling pathway (Mills *et al.*, 2018). Remarkably, local differences in the behavior of MT plus ends between areas of low and high MT densities were still observed in cells treated with the Rac1 inhibitors. Plus ends of MTs displayed dynamic instability at cell margins in MT-filled areas of the cytoplasm and robust growth in MT-depleted areas located distal to the barrier (Figure 4B, left; and Supplemental Videos S7 and S8). Tracking MT plus ends confirmed that in cells with inhibited Rac1 activity, similar to control cells, negative values of growth rates were frequent in areas of cytoplasm densely populated with MTs but were extremely rare in sparsely populated areas (Figure 4B, middle and right). Taken together, our results indicate that lack of MT catastrophes in areas of reduced MT density is not explained by local activation of the Rac1 signaling pathway.

DISCUSSION

In this study, we described a remarkable correlation between the local density of MTs in the cytoplasm and the dynamic behavior of MT plus ends. We found that at high local density MT plus ends undergo frequent catastrophes, whereas at low density they persistently grow and almost never shorten. The simplest explanation for our observations would involve a gradient of free tubulin subunits. Results of in vitro studies indicate that the frequency of catastrophes drops with an increase in the concentration of free tubulin subunits (Walker *et al.*, 1988), and therefore elevated tubulin subunit levels could explain the lack of catastrophes in areas of cytoplasm with low MT density. However, our FCS measurements indicate that the level of free tubulin subunits is uniform throughout the cytoplasm. Thus, the MT density–dependent switching of MT behavior is not determined by the concentration of free tubulin subunits. Our observations are in line with results of studies of a γ-tubulin–associated protein mutation in fission yeast (Zimmerman and Chang, 2005). Mutant cells had fewer than normal MTs with catastrophe defects that could not be explained by an increase in concentration of free tubulin dimers (Zimmerman and Chang, 2005). An alternative hypothesis is that differences in behavior of MT plus ends are explained by local variations in the concentration of regulatory factors that directly or indirectly control MT dynamics. We propose two possible mechanisms that explain persistent growth of MTs in areas of cytoplasm with low MT density and frequent catastrophes in the high MT density areas (Figure 5).

The first potential mechanism assumes that MT walls provide binding platforms for regulatory molecules that negatively affect the activities of protein factors stabilizing MTs (Figure 5A) and/or positively influence the activities of catastrophe-promoting factors. Protein factors that control MT dynamics are generally regulated by phosphorylation (Drewes *et al.*, 1998; Cassimeris and Spittle, 2001; Cassimeris, 2002; Akhmanova and Steinmetz, 2008; Holmfeldt *et al.*, 2009; Lyle *et al.*, 2009). We therefore hypothesize that regulatory molecules scaffolded on the surface of MTs could be protein kinases and phosphatases. In support of this hypothesis, numerous protein kinases and phosphatases were found to directly or indirectly bind MTs (Ookata *et al.*, 1995; Sontag *et al.*, 1995; Liao *et al.*, 1998; Nagata *et al.*, 1998; Burgess and Reiner, 2000; Yamada *et al.*, 2000), and inhibitors of their activities induced rapid changes in MT dynamic instability in living cells (Howell *et al.*, 1997). A high surface area of MTs in densely populated areas of the cytoplasm would result in a high concentration of binding sites for regulatory molecules and therefore create local areas of elevated protein kinase and/or phosphatase activities. Protein kinases could increase MT catastrophes by phosphorylating MT-stabilizing protein factors, such as structural MT-associated proteins (MAPs) (Mandell and Banker, 1996; Drewes *et al.*, 1998; Gundersen and Cook, 1999), including ubiquitously expressed MAP4 (Bulinski and Borisy, 1980). Phosphorylation of MT-binding domains of MAPs is well known to reduce their binding to MTs and therefore their ability to suppress catastrophes (Illenberger *et al.*, 1996; Shiina and Tsukita, 1999). Likewise, MT-bound protein phosphatases could dephosphorylate catastrophe-promoting cytosolic proteins, such as Op18/stathmin, increasing their activities (Cassimeris, 2002; Holmfeldt *et al.*, 2009). In support of this idea, the existence of gradients of phosphorylated Op18/stathmin in cells has been demonstrated experimentally

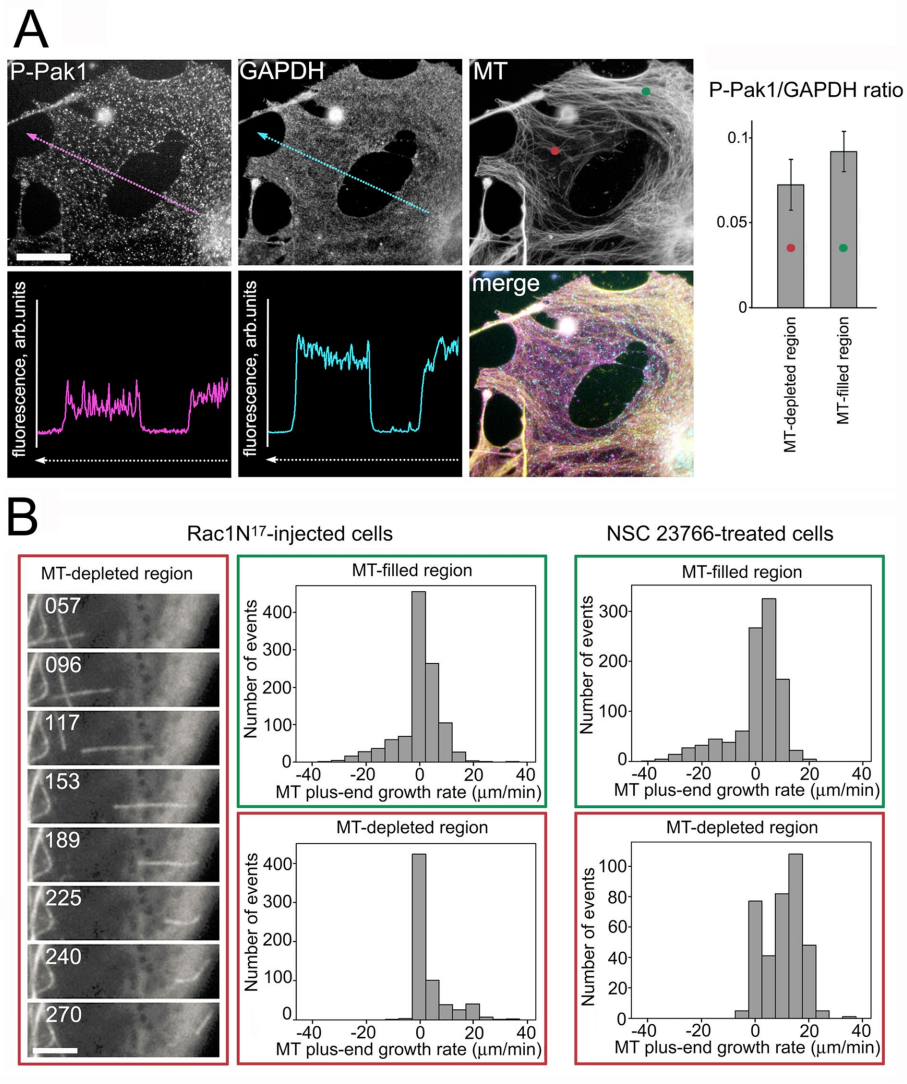

FIGURE 4: The lack of catastrophes in areas of cytoplasm with low MT density cannot be explained by local activation of the Rac1 signaling pathway. (A) Left panel, images of an NIH3T3 fibroblast with a microsurgically produced barrier triple-immunostained with antibodies against phosphorylated Pak1 (P-Pak1, top left), GAPDH (top, middle), and tubulin (MT, top right); dotted lines in the top left and middle images indicate positions of line scans of fluorescence intensity profiles shown in the bottom left and middle images; bottom right, merged image of fluorescence of phosphorylated Pak1 (color coded in magenta), GAPDH (color coded in cyan), and tubulin (color coded in yellow). Bar, 30 µm. Right panel, bar chart of phosphorylated Pak1/GAPDH fluorescence ratios measured in the MT-depleted area distal to the barrier and a MT-filled area at the cell margin (marked by red and green dots, respectively, in the top right image of left panel). Intensity of fluorescence of phosphorylated Pak1 is not increased in the area of cytoplasm distal to the barrier, which indicates that Pak1 is not activated locally in this area. (B) MT plus-end dynamics in areas of low and high MT densities in fish melanophores with Rac1activity inhibited by microinjection of recombinant dominant-negative mutant protein $Rac1N^{17}$(left and middle panels) or treatment with membrane-permeable inhibitor NSC 23766 (right panels); left panel, sequential images of a MT located distal to the barrier in a $Rac1N^{17}$-injected cell; numbers indicate time in seconds; bar, 5 µm; left and middle panels, histograms of MT growth rates (measured as displacement of MT plus ends within 5 s time intervals) in MT-filled areas of cytoplasm located at the cell margin (top) or MT-depleted areas distal to the barrier (bottom) in cells with Rac1 activity inhibited by microinjection with $Rac1N^{17}$solution (middle panel) or treated with NSC 23766. The sparsity of negative values of plus-end growth rates distal to the barrier indicates that persistent growth of MTs does not require local activation of Rac1.

(Andersen *et al.*, 1997). Theoretical studies indicate that spatially segregated protein kinase/phosphatase systems can generate steady state phospho-state gradients of rapidly diffusing molecules (Lipkow and Odde, 2008). Therefore accumulation of protein kinases and phosphatases in areas of high MT density may create a phosphoprotein environment that enhances MT catastrophes.

The second potential mechanism involves competition of MTs for factors that promote assembly and suppress catastrophes. These factors may bind to growing plus ends (Figure 5B, top) or along the length (Figure 5B, bottom) of MTs. Competition of MT tips for stabilizing factors was recently proposed to explain a negative correlation between MT growth rates and plus-end density in droplets of *Xenopus* egg extract confined in engineered microscopic chambers in vitro (Geisterfer *et al.*, 2020). In this system, each growing MT plus end apparently acted as a sink for key regulators of MT growth. Increasing the number of plus ends in the egg extract caused local depletion of protein factors essential for MT growth, leading to a decrease in the growth rate. Likewise, in our study a depletion of MT assembly–promoting factors by the accumulation of plus ends in specific regions of the cytoplasm, such as the cell margin, could cause catastrophes. The identity of local assembly-promoting factors that protect MT plus ends from disassembly is not known. Good candidates are plus-end tracking proteins EB1 and EB3 that support persistent MT growth by suppressing catastrophes (Rogers *et al.*, 2002; Komarova *et al.*, 2009). However, a recent in vitro study suggests that combinatory effects of several protein factors are required to promote fast and sustained plus-end growth (Arpag *et al.*, 2020). Therefore other proteins may also be involved such as CLASP2, which suppresses microtubule catastrophes and promotes rescue (Lawrence *et al.*, 2018), CLIP170, which is also known to function as a MT rescue factor (Komarova *et al.*, 2002), and XMAP215, which catalyzes the addition of individual tubulin subunits to the growing MT ends (Al-Bassam *et al.*, 2010). Likewise, MTs may compete for stabilizing factors that bind along their length (Figure 5B, bottom), such as structural MAPs, including MAP2, MAP4, and doublecortin that decorate the MT lattice and strongly suppress MT catastrophes (van der Vaart *et al.*, 2009; Goodson and Jonasson, 2018). Soluble pools of these factors may be exhausted at high density of MTs, causing a local increase in catastrophe frequency, whereas at low MT density these factors could saturate MT walls, leading to sustained growth. Regardless of the mechanism of MT stabilization, an expected property of putative regulators of local MT dynamics is slow diffusion that would allow maintenance of a standing gradient of their concentration in the cytoplasm.

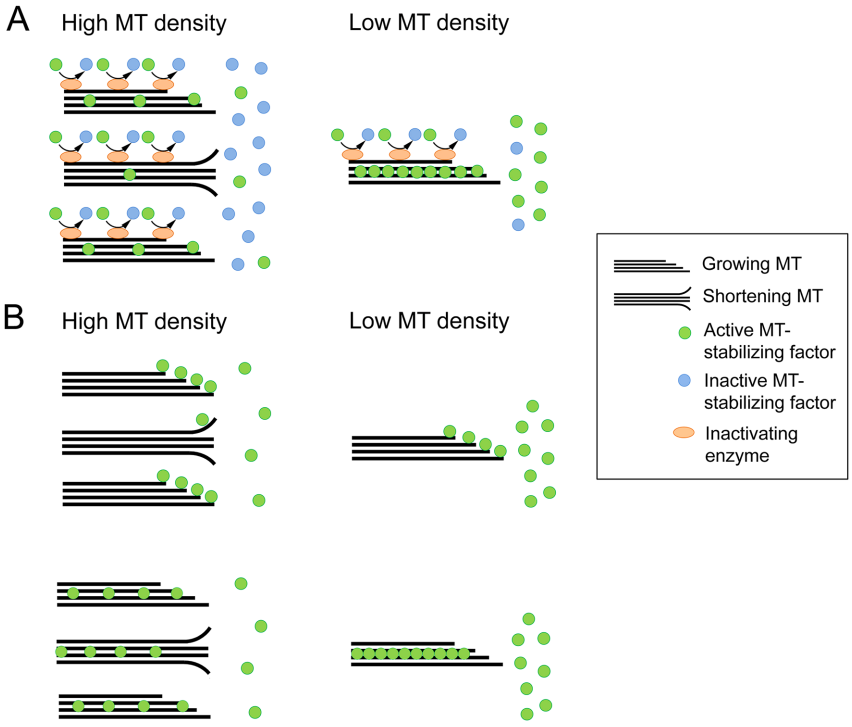

FIGURE 5: Hypotheses to explain the role of MT density in regulating MT dynamics. (A) MTs (black lines) scaffold regulatory enzymes (orange ovals), such as protein kinases or phosphatases, which inactivate MT-stabilizing protein factors (green and blue circles, active and inactive factors, respectively) by preventing their binding to MTs; at high MT density (left), the local concentration of regulatory enzymes is high, MT-stabilizing factors are mostly inactive, and some MTs undergo catastrophes and shorten (a set of straight and curved black lines); at low MT density (right) the concentration of regulatory enzymes is low, MT-stabilizing factors are active, and MTs never shorten. (B) MTs compete for stabilizing factors (green circles) that bind to plus ends of growing MTs (top; sets of straight lines) or along the MT length (bottom); at high MT density (left), competition leads to a local decrease in concentration of MT-stabilizing factors, leading to emergence of shortening MTs (sets of straight and curved black lines); at low MT density (right) the concentration of MT-stabilizing factors is high and MTs never shorten.

In conclusion, our data indicate that the default mode of plus-end behavior at low MT density is persistent growth. Increased MT density changes the balance between activities of MT-stabilizing and -destabilizing factors, leading to the initiation of MT catastrophes and dynamic instability. We believe that uninterrupted growth at low density is a fundamental property of MTs that allows them to promptly fill nascent areas of the cytoplasm in cells that rapidly change shape. Such basic behavior of MTs is further amplified by signaling mechanisms activated during particular cellular events, such as migration, in which sustained MT growth is maintained through Rac1-dependent signaling at the advancing cell leading edge (Wittmann *et al.*, 2003). Understanding the molecular details of regulation MT dynamics observed in our experiments is an exciting line of further investigation.

MATERIALS AND METHODS

Request a protocol through *Bio-protocol*.

Cell cultures, microinjection, and microsurgery

Cultures of black tetra melanophores were prepared as described previously (Ikeda *et al.*, 2010). Removal of scales was performed according to the protocol approved by the institutional animal care and use committee (UConn Health, IACUC protocol number 102021-0122). Melanophores were cultured on carbon-coated coverslips at 27°C in DMEM buffered with 20 mM HEPES (MilliporeSigma, Burlington, MA) supplemented with 20% fetal calf serum (Life Technologies, Carlsbad, CA), 100 IU/ml penicillin, 0.12 mg/ml streptomycin, and 0.1 mg/ml gentamicin. Aggregation of pigment granules was induced by 10^{-5} M adrenalin (MilliporeSigma, Burlington, MA). NIH3T3 fibroblasts (American Type Culture Collection; CRL-1658) were cultured in DMEM supplemented with 10% calf serum (Life Technologies, Carlsbad, CA), 100 IU/ml penicillin, and 0.12 mg/ml streptomycin. Normal human skin fibroblasts (Cornell Institute; catalogue number GM00498, passage 25) were grown in MEM supplemented with 15% fetal bovine serum (Life Technologies, Carlsbad, CA), 100 IU/ml penicillin, and 0.12 mg/ml streptomycin. To increase cell size, NIH3T3 and normal human skin fibroblasts were treated with mitomycin C (10 µg/ml; MilliporeSigma, Burlington, MA) for 3–5 d. For fluorescence labeling of MTs, cells were injected with bovine brain tubulin conjugated with Cy3 as described in detail previously (Ikeda *et al.*, 2010). After microinjection, cells were kept for ~60 min at 30°C (fish melanophores) or 37°C (mammalian fibroblasts) for incorporation of labeled tubulin into microtubules. Microsurgery was performed with a glass microneedle as described previously (Ikeda *et al.*, 2010).

Acquisition of images of MTs and analysis of MT dynamics

Fluorescence microscopy of MTs in melanophores and fibroblasts was performed using a Nikon TiE inverted microscope equipped with a Plan Apo x100 1.4 NA objective lens. Fluorescence images were acquired with an Andor iXon EM-CCD camera (Andor Technology, Windsor, CT) driven by Metamorph image acquisition and analysis software (Universal Imaging, Downington, PA). Live imaging of cells injected with Cy3-tubulin was performed in the presence of the oxygen scavenger Oxyrase (Oxyrase Company, Mansfield, OH) to reduce photodamage (Ikeda *et al.*, 2010).

MT dynamics were measured by acquiring time series of images of Cy3-labeled MTs and manually tracking individual MT ends using Metamorph software. Parameters of MT dynamic instability were determined as described previously (Vorobjev *et al.*, 2001).

Treatment of cells with Rac1 inhibitors

To inhibit Rac1 activity, cells were treated for 60–120 min with Rac1 inhibitor NSC23766 (50 µM; Bio-Techne Corporation, Minneapolis, MN) or microinjected with recombinant dominant-negative mutant Rac1 protein (Ridley *et al.*, 1992) (needle concentration 5 mg/ml) as described in Waterman-Storer *et al.* (1999).

Measurement ratios of free tubulin subunit concentrations in areas of cytoplasm with high and low MT densities

Ratios of concentrations of free tubulin subunits in areas of cytoplasm with high and low MT densities were determined using fluorescence ratiometric imaging or FCS.

For fluorescence ratiometric imaging, melanophores were coinjected with bovine brain tubulin labeled with Cy3 and a volume

maker Alexa Fluor 488–dextran (needle concentration 200 μM; Thermo Fisher Scientific, Waltham, MA). Images of cells were acquired using rhodamine (for fluorescence of Cy3-tubulin) and fluorescein (for Alexa Fluor 488–dextran fluorescence) filter sets, and integrated fluorescence was measured in each channel in the same areas located between MTs using MetaMorph image acquisition and analysis software (Molecular Devices, Downington, PA). Measurements were performed in the same cells in regions of cytoplasm with high and low MT densities. After subtracting background fluorescence (measured in each channel outside the cells), the values of Cy3 fluorescence were normalized for Alexa Fluor 488 fluorescence determined for the same regions. The data were used to calculate the ratios of normalized Cy3 fluorescence determined in the same cells for areas of low and high MT densities.

For FCS measurements of local concentrations and diffusion coefficients of tubulin subunits, NIH3T3 fibroblasts were transfected with plasmid DNA encoding EGFP–tubulin (a gift from Anna Akhmanova, Utrecht University) using GeneCellin DNA transfection reagent (Bulldog Bio, Portsmouth, NH). Imaging of transfected cells and FCS measurements were performed with an LSM 510-ConfoCor 3 attached to an Axiovert 100 M microscope with C-Apochromat 40x, 1.2 NA water immersion objective lens. FCS measurements were performed in seven different cells with the FCS observation volume positioned at two separate locations within the high MT–density regions and at two separate locations within the low MT–density regions. FCS autocorrelation functions determined at each location were fitted using the equation for three-dimensional diffusion (Eq. 1) as described previously (Paradise *et al.*, 2007):

$$G(t)=\left(1+\frac{y_t e^{-t/\tau_t}}{1-y_t}\right)\frac{1}{N}\sum_{i=1}^{CN}\frac{y_i}{\left(1+\frac{t}{\tau_i}\right)\sqrt{1+\frac{\omega^2 t}{\tau^i}}} \quad (1)$$

where $G(t)$ is the autocorrelation, N is the average number of diffusing molecules in the FCS observation volume, y is the fraction of each component, and τ is the diffusion time for each component. Initially the autocorrelation data were fitted using a single-component model. However, with the single -component model the fit deviation profiles revealed significant deviation at slower τ values and unacceptably large overall χ^2 values. Accordingly, the autocorrelation data were fitted using a two-component model. With the two-component model the fit deviation profiles no longer revealed significant deviations and the overall χ^2 values were reduced on average 4.2 ± 0.6-fold compared with the single-component model. This suggests that cells contain two different components of exogenous EGFP–tubulin with distinct concentrations and diffusion coefficients. Accordingly, all FCS autocorrelation data were fitted with a two-component model.

The diffusion coefficient (D) for each component was derived from the τ value according to Eq. 2:

$$\tau=\omega_1^2/4D \quad (2)$$

where ω_1 is the radius of the FCS observation volume.

The concentration (c) for each component was derived from the average number of diffusing molecules (N) in the FCS observation volume according to Eq. 3:

$$C=\frac{N}{(N_A)(V)} \quad (3)$$

where N_A is Avogadro's number and V is the FCS observation volume.

The diffusion coefficient for the fast component of tubulin (12.6 ± 6.3 μm^2/s; mean ± SD, n = 28 measurements in seven different cells) is slightly larger than the previously published overall diffusion coefficients for tubulin in live cells (D = 6 μm^2/s; Wang *et al.*, 2004). The explanation for this discrepancy may be related to the number of components in the model used to fit the FCS autocorrelation function. The previously reported diffusion coefficient apparently represents an overall value derived using a one-component model to fit all the FCS autocorrelation data (close inspection of the previously published autocorrelation data reveals minor fit deviation at slower τ values). In the studies reported here a two-component model provided a better overall fit for the autocorrelation data, resolving both a fast component and a slow component with different diffusion coefficients. The diffusion coefficient for the fast component by itself is slightly larger than the previously reported overall diffusion coefficient, while the diffusion coefficient for the slow component is much smaller (0.003 ± 0.004 μm^2/s). If the diffusion coefficients for both the fast and slow components were combined, the overall diffusion coefficient for the studies reported here would be similar to the previously published value. We believe that the diffusion coefficient for the fast component reported here may provide a more accurate estimate of the actual diffusion coefficient for freely diffusing tubulin in live cells, without the confounding effects of the slow component, which may not represent freely diffusing tubulin.

Comparison of actin filament levels in MT-depleted areas of cytoplasm distal to barriers and cell margins

To compare levels of actin filaments in areas of cytoplasm distal to the barrier and intact cell margins, mitomycin-treated NIH3T3 fibroblasts were microinjected with volume marker Oregon Green 488–labeled fixable dextran (needle concentration 100 μg/ml; Thermo Fisher Scientific, Waltham, MA) and after microsurgery fixed with paraformaldehyde. Cell were then permeabilized with 0.1% Triton X-100, blocked with 1% bovine serum albumin, and sequentially incubated with TRITC-phalloidin (0.1 μM; MilliporeSigma, Burlington, MA) mouse monoclonal antibody against alpha-tubulin (DM1A; ThermoFisher Scientific, Waltham, MA; 0.5 μg/ml), and goat anti-mouse antibody conjugated with Cy5 (Jackson ImmunoResearch, West Grove, PA; 5 μg/ml) for fluorescent staining of actin filaments and MTs. Seven cells with reduced MT density distal to microsurgically produced wounds were selected for the measurement of dextran and phalloidin fluorescence acquired using relevant filter sets. TRITC and Oregon Green 488 fluorescence were quantified using Metamorph Region Measurement Tool in ~20 μm circular regions of interest placed over areas of cytoplasm distal to the barrier and at the cell margin. After background subtraction, the relative fluorescence of actin filaments was determined for each region of interest by dividing values of TRITC fluorescence by Oregon Green 488 fluorescence. Relative actin filament fluorescence ratios were then calculated by dividing values determined for the same cells in low MT density areas and cell margins (Supplemental Figure 2).

Comparison of phosphorylated Pak1 levels in areas of cytoplasm with low and high MT densities

To compare levels of phosphorylated Pak1 in areas of cytoplasm sparsely and densely populated with MTs, mitomycin-treated NIH3T3 fibroblasts with a microsurgically generated wound were fixed with 4% paraformaldehyde for 30 min, permeabilized with 0.1% Triton X-100, and blocked with 1% bovine serum albumin. Cells were then triple-immunostained with antibodies against phosphorylated Pak1 (to quantify local levels of phosphorylated Pak1), tubulin (for verification of MT density), and GAPDH (used as a

cytoplasm volume marker). Immunostaining was performed by sequential incubation of fixed cells with the following primary and secondary antibodies: rabbit antibody against phosphorylated Pak1 (S199/204; Cell Signaling Technology, Danvers, MA; 1:200), mouse monoclonal antibody against alpha-tubulin (DM1A; ThermoFisher Scientific, Waltham, MA; 0.5 µg/ml), chicken anti-GAPDH antibody (ab83956; Abcam, Cambridge, MA; 2.5 µg/ml), goat anti-rabbit antibody conjugated with Alexa 488 (ThermoFisher Scientific, Waltham, MA; 5 µg/ml), goat anti-mouse antibody conjugated with Cy5 (Jackson ImmunoResearch, West Grove, PA; 5 µg/ml), and rhodamine-conjugated goat anti-chicken antibody (Jackson ImmunoResearch, West Grove, PA; 5 µg/ml). Phosphorylated Pak1 and GAPDH fluorescence was quantified in 10 µm circular regions of interest in the same regions of cytoplasm using the MetaMorph Region Measurement Tool. After background subtraction, ratios of phosphorylated Pak1/GAPDH fluorescence were calculated for each cell. Data for 10 cells were averaged and used to generate the bar chart shown in Figure 4A.

ACKNOWLEDGMENTS

This work was supported by National Institutes of Health grants GM62290 to V. R., GM117061 to Y. W., and NS99730 to J. C. I. V. is supported by grants AP08857554 (Ministry of Education and Science [MES], Kazakhstan) and ORAU 240919FD3937 (Nazarbayev University). We thank Gary Borisy (Forsyth Institute) for insightful discussions and critical reading of the manuscript.

REFERENCES

Akhmanova A, Hoogenraad CC, Drabek K, Stepanova T, Dortland B, Verkerk T, Vermeulen W, Burgering BM, De Zeeuw CI, Grosveld F, Galjart N (2001). Clasps are CLIP-115 and -170 associating proteins involved in the regional regulation of microtubule dynamics in motile fibroblasts. Cell 104, 923–935.

Akhmanova A, Steinmetz MO (2008). Tracking the ends: a dynamic protein network controls the fate of microtubule tips. Nat Rev Mol Cell Biol 9, 309–322.

Akhmanova A, Steinmetz MO (2015). Control of microtubule organization and dynamics: two ends in the limelight. Nat Rev Mol Cell Biol 16, 711–726.

Al-Bassam J, Kim H, Brouhard G, van Oijen A, Harrison SC, Chang F (2010). CLASP promotes microtubule rescue by recruiting tubulin dimers to the microtubule. Dev Cell 19, 245–258.

Andersen SS, Ashford AJ, Tournebize R, Gavet O, Sobel A, Hyman AA, Karsenti E (1997). Mitotic chromatin regulates phosphorylation of Stathmin/Op18. Nature 389, 640–643.

Arpag G, Lawrence EJ, Farmer VJ, Hall SL, Zanic M (2020). Collective effects of XMAP215, EB1, CLASP2, and MCAK lead to robust microtubule treadmilling. Proc Natl Acad Sci USA 117, 12847–12855.

Braun A, Dang K, Buslig F, Baird MA, Davidson MW, Waterman CM, Myers KA (2014). Rac1 and Aurora A regulate MCAK to polarize microtubule growth in migrating endothelial cells. J Cell Biol 206, 97–112.

Bulinski JC, Borisy GG (1980). Widespread distribution of a 210,000 mol wt microtubule-associated protein in cells and tissues of primates. J Cell Biol 87, 802–808.

Burgess HA, Reiner O (2000). Doublecortin-like kinase is associated with microtubules in neuronal growth cones. Mol Cell Neurosci 16, 529–541.

Cassimeris L (2002). The oncoprotein 18/stathmin family of microtubule destabilizers. Curr Opin Cell Biol 14, 18–24.

Cassimeris L, Spittle C (2001). Regulation of microtubule-associated proteins. Int Rev Cytol 210, 163–226.

Caviston JP, Holzbaur EL (2006). Microtubule motors at the intersection of trafficking and transport. Trends Cell Biol 16, 530–537.

Chong C, Tan L, Lim L, Manser E (2001). The mechanism of PAK activation. Autophosphorylation events in both regulatory and kinase domains control activity. J Biol Chem 276, 17347–17353.

Daub H, Gevaert K, Vandekerckhove J, Sobel A, Hall A (2001). Rac/Cdc42 and p65PAK regulate the microtubule-destabilizing protein stathmin through phosphorylation at serine 16. J Biol Chem 276, 1677–1680.

Desai A, Mitchison TJ (1997). Microtubule polymerization dynamics. Annu Rev Cell Dev Biol 13, 83–117.

Dharmawardhane S, Brownson D, Lennartz M, Bokoch GM (1999). Localization of p21-activated kinase 1 (PAK1) to pseudopodia, membrane ruffles, and phagocytic cups in activated human neutrophils. J Leukoc Biol 66, 521–527.

Drewes G, Ebneth A, Mandelkow EM (1998). MAPs, MARKs and microtubule dynamics. Trends Biochem Sci 23, 307–311.

Etienne-Manneville S (2013). Microtubules in cell migration. Annu Rev Cell Dev Biol 29, 471–499.

Gao Y, Dickerson JB, Guo F, Zheng J, Zheng Y (2004). Rational design and characterization of a Rac GTPase-specific small molecule inhibitor. Proc Natl Acad Sci USA 101, 7618–7623.

Gatti A, Huang Z, Tuazon PT, Traugh JA (1999). Multisite autophosphorylation of p21-activated protein kinase gamma-PAK as a function of activation. J Biol Chem 274, 8022–8028.

Geisterfer ZM, Zhu DY, Mitchison TJ, Oakey J, Gatlin JC (2020). Microtubule growth rates are sensitive to global and local changes in microtubule plus-end density. Curr Biol 30, 3016–3023.e3013.

Goodson HV, Jonasson EM (2018). Microtubules and microtubule-associated proteins. Cold Spring Harb Perspect Biol 10, a022608.

Gundersen GG, Cook TA (1999). Microtubules and signal transduction. Curr Opin Cell Biol 11, 81–94.

Hayden JH, Bowser SS, Rieder CL (1990). Kinetochores capture astral microtubules during chromosome attachment to the mitotic spindle: direct visualization in live newt lung cells. J Cell Biol 111, 1039–1045.

Heald R, Khodjakov A (2015). Thirty years of search and capture: the complex simplicity of mitotic spindle assembly. J Cell Biol 211, 1103–1111.

Holmfeldt P, Sellin ME, Gullberg M (2009). Predominant regulators of tubulin monomer-polymer partitioning and their implication for cell polarization. Cell Mol Life Sci 66, 3263–3276.

Howell B, Odde DJ, Cassimeris L (1997). Kinase and phosphatase inhibitors cause rapid alterations in microtubule dynamic instability in living cells. Cell Motil Cytoskeleton 38, 201–214.

Ikeda K, Semenova I, Zhapparova O, Rodionov V (2010). Melanophores for microtubule dynamics and motility assays. Methods Cell Biol 97, 401–414.

Illenberger S, Drewes G, Trinczek B, Biernat J, Meyer HE, Olmsted JB, Mandelkow EM, Mandelkow E (1996). Phosphorylation of microtubule-associated proteins MAP2 and MAP4 by the protein kinase p110mark. Phosphorylation sites and regulation of microtubule dynamics. J Biol Chem 271, 10834–10843.

Janson ME, de Dood ME, Dogterom M (2003). Dynamic instability of microtubules is regulated by force. J Cell Biol 161, 1029–1034.

Keating TJ, Peloquin JG, Rodionov VI, Momcilovic D, Borisy GG (1997). Microtubule release from the centrosome. Proc Natl Acad Sci USA 94, 5078–5083.

Knaus UG, Bokoch GM (1998). The p21Rac/Cdc42-activated kinases (PAKs). Int J Biochem Cell Biol 30, 857–862.

Komarova Y, De Groot CO, Grigoriev I, Gouveia SM, Munteanu EL, Schober JM, Honnappa S, Buey RM, Hoogenraad CC, Dogterom M, *et al.* (2009). Mammalian end binding proteins control persistent microtubule growth. J Cell Biol 184, 691–706.

Komarova YA, Akhmanova AS, Kojima S, Galjart N, Borisy GG (2002). Cytoplasmic linker proteins promote microtubule rescue in vivo. J Cell Biol 159, 589–599.

Kumar P, Lyle KS, Gierke S, Matov A, Danuser G, Wittmann T (2009). GSK-3beta phosphorylation modulates CLASP-microtubule association and lamella microtubule attachment. J Cell Biol 184, 895–908.

Lane J, Allan V (1998). Microtubule-based membrane movement. Biochim Biophys Acta 1376, 27–55.

Lawrence EJ, Arpag G, Norris SR, Zanic M (2018). Human CLASP2 specifically regulates microtubule catastrophe and rescue. Mol Biol Cell 29, 1168–1177.

Liao H, Li Y, Brautigan DL, Gundersen GG (1998). Protein phosphatase 1 is targeted to microtubules by the microtubule-associated protein Tau. J Biol Chem 273, 21901–21908.

Lipkow K, Odde DJ (2008). Model for protein concentration gradients in the cytoplasm. Cell Mol Bioeng 1, 84–92.

Lomakin AJ, Semenova I, Zaliapin I, Kraikivski P, Nadezhdina E, Slepchenko BM, Akhmanova A, Rodionov V (2009). CLIP-170-dependent capture of membrane organelles by microtubules initiates minus-end directed transport. Dev Cell 17, 323–333.

Lyle K, Kumar P, Wittmann T (2009). SnapShot: Microtubule regulators I. Cell 136, 380–380.e381.

Mandell JW, Banker GA (1996). Microtubule-associated proteins, phosphorylation gradients, and the establishment of neuronal polarity. Perspect Dev Neurobiol 4, 125–135.

Mills SC, Howell L, Beekman A, Stokes L, Mueller A (2018). Rac1 plays a role in CXCL12 but not CCL3-induced chemotaxis and Rac1 GEF inhibitor NSC23766 has off target effects on CXCR4. Cell Signal 42, 88–96.
Mitchison T, Kirschner M (1984). Dynamic instability of microtubule growth. Nature 312, 237–242.
Murphy DB, Tilney LG (1974). The role of microtubules in the movement of pigment granules in teleost melanophores. J Cell Biol 61, 757–779.
Nagata K, Puls A, Futter C, Aspenstrom P, Schaefer E, Nakata T, Hirokawa N, Hall A (1998). The MAP kinase kinase kinase MLK2 co-localizes with activated JNK along microtubules and associates with kinesin superfamily motor KIF3. EMBO J 17, 149–158.
Odde DJ (1997). Estimation of the diffusion-limited rate of microtubule assembly. Biophys J 73, 88–96.
Ookata K, Hisanaga S, Bulinski JC, Murofushi H, Aizawa H, Itoh TJ, Hotani H, Okumura E, Tachibana K, Kishimoto T (1995). Cyclin B interaction with microtubule-associated protein 4 (MAP4) targets p34cdc2 kinase to microtubules and is a potential regulator of M-phase microtubule dynamics. J Cell Biol 128, 849–862.
Paradise A, Levin MK, Korza G, Carson JH (2007). Significant proportions of nuclear transport proteins with reduced intracellular mobilities resolved by fluorescence correlation spectroscopy. J Mol Biol 356, 50–65.
Ridley AJ, Paterson HF, Johnston CL, Diekmann D, Hall A (1992). The small GTP-binding protein rac regulates growth factor-induced membrane ruffling. Cell 70, 401–410.
Rodionov V, Nadezhdina E, Borisy G (1999). Centrosomal control of microtubule dynamics. Proc Natl Acad Sci USA 96, 115–120.
Rodionov VI, Borisy GG (1997a). Microtubule treadmilling in vivo. Science 275, 215–218.
Rodionov VI, Borisy GG (1997b). Self-centring activity of cytoplasm. Nature 386, 170–173.
Rodionov VI, Gyoeva FK, Gelfand VI (1991). Kinesin is responsible for centrifugal movement of pigment granules in melanophores. Proc Natl Acad Sci USA 88, 4956–4960.
Rodionov VI, Hope AJ, Svitkina TM, Borisy GG (1998). Functional coordination of microtubule-based and actin-based motility in melanophores. Curr Biol 8, 165–168.
Rodionov VI, Lim SS, Gelfand VI, Borisy GG (1994). Microtubule dynamics in fish melanophores. J Cell Biol 126, 1455–1464.
Rogers SL, Rogers GC, Sharp DJ, Vale RD (2002). Drosophila EB1 is important for proper assembly, dynamics, and positioning of the mitotic spindle. J Cell Biol 158, 873–884.
Salmon ED, Saxton WM, Leslie RJ, Karow ML, McIntosh JR (1984). Diffusion coefficient of fluorescein-labeled tubulin in the cytoplasm of embryonic cells of a sea urchin: video image analysis of fluorescence redistribution after photobleaching. J Cell Biol 99, 2157–2164.
Sells MA, Pfaff A, Chernoff J (2000). Temporal and spatial distribution of activated Pak1 in fibroblasts. J Cell Biol 151, 1449–1458.
Shiina N, Tsukita S (1999). Mutations at phosphorylation sites of Xenopus microtubule-associated protein 4 affect its microtubule-binding ability and chromosome movement during mitosis. Mol Biol Cell 10, 597–608.
Sontag E, Nunbhakdi-Craig V, Bloom GS, Mumby MC (1995). A novel pool of protein phosphatase 2A is associated with microtubules and is regulated during the cell cycle. J Cell Biol 128, 1131–1144.
Vale RD (2003). The molecular motor toolbox for intracellular transport. Cell 112, 467–480.
van der Vaart B, Akhmanova A, Straube A (2009). Regulation of microtubule dynamic instability. Biochem Soc Trans 37, 1007–1013.
Vorobjev I, Malikov V, Rodionov V (2001). Self-organization of a radial microtubule array by dynein-dependent nucleation of microtubules. Proc Natl Acad Sci USA 98, 10160–10165.
Wadsworth P (1999). Regional regulation of microtubule dynamics in polarized, motile cells. Cell Motil Cytoskeleton 42, 48–59.
Walczak CE, Heald R (2008). Mechanisms of mitotic spindle assembly and function. Int Rev Cytol 265, 111–158.
Walker RA, O'Brien ET, Pryer NK, Soboeiro MF, Voter WA, Erickson HP, Salmon ED (1988). Dynamic instability of individual microtubules analyzed by video light microscopy: rate constants and transition frequencies. J Cell Biol 107, 1437–1448.
Wang Z, Shah JV, Chen Z, Sun CH, Berns MW (2004). Fluorescence correlation spectroscopy investigation of a GFP mutant-enhanced cyan fluorescent protein and its tubulin fusion in living cells with two-photon excitation. J Biomed Opt 9, 395–403.
Waterman-Storer CM, Salmon ED (1997). Actomyosin-based retrograde flow of microtubules in the lamella of migrating epithelial cells influences microtubule dynamic instability and turnover and is associated with microtubule breakage and treadmilling. J Cell Biol 139, 417–434.
Waterman-Storer CM, Worthylake RA, Liu BP, Burridge K, Salmon ED (1999). Microtubule growth activates Rac1 to promote lamellipodial protrusion in fibroblasts. Nat Cell Biol 1, 45–50.
Welte MA (2004). Bidirectional transport along microtubules. Curr Biol 14, R525–R537.
Wittmann T, Bokoch GM, Waterman-Storer CM (2003). Regulation of leading edge microtubule and actin dynamics downstream of Rac1. J Cell Biol 161, 845–851.
Wittmann T, Bokoch GM, Waterman-Storer CM (2004). Regulation of microtubule destabilizing activity of Op18/stathmin downstream of Rac1. J Biol Chem 279, 6196–6203.
Wittmann T, Waterman-Storer CM (2001). Cell motility: can Rho GTPases and microtubules point the way? J Cell Sci 114, 3795–3803.
Wittmann T, Waterman-Storer CM (2005). Spatial regulation of CLASP affinity for microtubules by Rac1 and GSK3beta in migrating epithelial cells. J Cell Biol 169, 929–939.
Wu YI, Frey D, Lungu OI, Jaehrig A, Schlichting I, Kuhlman B, Hahn KM (2009). A genetically encoded photoactivatable Rac controls the motility of living cells. Nature 461, 104–108.
Yamada T, Aoyama Y, Owada MK, Kawakatsu H, Kitajima Y (2000). Scraped-wounding causes activation and association of C-Src tyrosine kinase with microtubules in cultured keratinocytes. Cell Struct Funct 25, 351–359.
Zimmerman S, Chang F (2005). Effects of γ-tubulin complex proteins on microtubule nucleation and catastrophe in fission yeast. Mol Biol Cell 16, 2719–2733.